


 Cite this: *Nanoscale*, 2023, **15**, 8141

 Received 28th January 2023,
Accepted 26th March 2023

DOI: 10.1039/d3nr00416c

rsc.li/nanoscale

A luminescent Cu₄ cluster film grown by electro-spray deposition: a nitroaromatic vapour sensor†

 Arijit Jana,^a B. K. Spoorthi,^a Akhil S. Nair,^b Ankit Nagar,^a Biswarup Pathak,^b Tomas Base^c and Thalappil Pradeep^a

We present the fabrication and use of a film of a carborane-thiol-protected tetranuclear copper cluster with characteristic orange luminescence using ambient electro-spray deposition (ESD). Charged microdroplets of the clusters produced by an electro-spray tip deposit the clusters at an air–water interface to form a film. Different microscopic and spectroscopic techniques characterized the porous surface structure of the film. Visible and rapid quenching of the emission of the film upon exposure to 2-nitrotoluene (2-NT) vapours under ambient conditions was observed. Density functional theory (DFT) calculations established the favourable binding sites of 2-NT with the cluster. Desorption of 2-NT upon heating recovered the original luminescence, demonstrating the reusability of the sensor. Stable emission upon exposure to different organic solvents and its quenching upon exposure to 2,4-dinitrotoluene and picric acid showed selectivity of the film to nitroaromatic species.

Selective and observable detection of nitroaromatic precursors, widely used for the synthesis of explosives, has received special attention due to increased concerns of security.^{1–3} Direct detection of such chemical entities using instrumental methods, such as mass spectrometry,⁴ surface-enhanced Raman spectroscopy,⁵ and sophisticated sensor arrays,⁶ requires expensive infrastructure and/or complicated sampling protocols. On the other hand, optical detection with organic and inorganic sensing materials, such as π electron-rich aromatic compounds,⁷ metal–organic frameworks,⁸ dendrimers,⁹ polymers,¹⁰ quantum dots,¹¹ and gold mesoflowers,¹² has been explored for reliable detection. Optical detection primar-

ily relies on visible changes of luminescence in terms of the emission brightness or colour of such materials upon exposure to the sensing materials. Atomically precise metal nanoclusters with tunable luminescence characteristics are versatile additions to this application.^{13–15} Such nanomaterials have specific multicolour luminescence properties due to electronic transitions within closely spaced quantized electronic energy levels.^{16–18} Modulation of luminescence by applying external stimuli, such as temperature,^{19,20} pressure,²¹ and electric potential,²² suggests a possibility to have sensing responses with molecules, particularly electron-deficient nitroaromatic compounds.²³

Detection of nitroaromatics in the gas/vapour phase is challenging compared to their detection in the condensed state, primarily due to their low volatility and a lack of efficient intermolecular interactions.^{24,25} Therefore, the preparation of luminescent vapour sensors with highly sensitive exposed surface area is an essential goal towards easy, fast and reliable sensors. However, fabrication of an active two-dimensional (2D) surface composed of ultra-small nanoclusters is challenging due to their reduced stability, inherent reactivity, unregulated aggregation behaviour and the lack of large order inter-cluster interactions.^{26,27} To overcome such challenges, we introduced the ESD technique, which generates solvated charged microdroplets of cluster ions in air by applying an electric potential.^{28,29} Soft landing of ions onto a transient water surface resulted in a sensitive 2D nanocluster assembled film. The ESD technique favours fast and soft aggregation of clusters at the air–water interface without using long chain ligands,³⁰ metal ions,³¹ mixed solvent systems,³² thermal annealing,³³ and gel forming agents.³⁴ In our earlier experiments, we had shown the advantages of this technique for the preparation of various nanomaterials, including metallic nanobrushes,³⁵ nanopyramids and platelets,³⁶ vertically aligned nanoplates,³⁷ annealed nanoparticle superstructures,³⁸ and other surface exposed nanostructures.³⁹

Here, we have fabricated a robust surface-activated film of a Cu₄@ICBT cluster, covered with an *ortho*-carborane 12-iodo

^aDepartment of Chemistry, DST Unit of Nanoscience (DST UNS) and Thematic Unit of Excellence (TUE), Indian Institute of Technology Madras, Chennai 600036, India. E-mail: pradeep@iitm.ac.in

^bDepartment of Chemistry, Indian Institute of Technology Indore (IIT Indore), Indore 453552, India. E-mail: biswarup@iiti.ac.in

^cDepartment of Synthesis, Institute of Inorganic Chemistry, The Czech Academy of Science 1001, Husinec – Rez, 25068, Czech Republic. E-mail: tbase@iic.acs.cz

† Electronic supplementary information (ESI) available. See DOI: <https://doi.org/10.1039/d3nr00416c>

9-thiol ligand, through the ESD technique. The atomic structure of the cluster shows a nearly square planar Cu_4 core protected by four carborane ligands along with three iodine atoms (shown in Fig. 1a).⁴⁰ $\text{Cu}_4@$ ICBT was synthesized by a ligand exchange-induced structure transformation (LEIST) reaction starting from the Cu_{18} nanocluster.⁴¹ LEIST synthesis reactions were used for preparing various gold⁴² and silver⁴³ nanoclusters. Synthetic details and structural characterization of the cluster were described previously⁴⁰ and the essential details are presented in Fig. S1 in the ESI.† ESD experiments were performed using a home-built setup. Fig. 1b shows the schematic representation of the ESD setup.

Details of the deposition process are presented in the ESI.† In brief, charged microdroplets of cluster ions were generated upon applying a high voltage (2.5–3 kV) through a platinum

(Pt) wire to a 0.5 mM solution of the cluster using a glass capillary (tip diameter, 25–30 μm) (shown in Fig. S2†). The deposition of ions was performed on water, which was grounded to neutralize the charge. After 30 min of deposition, we observed a white-coloured thin film floating on the water surface (shown in the inset of Fig. 1b and c), and this film was transferred onto either a clean glass slide or an Al foil for further experiments. The floating nature of the film is due to the hydrophobic nature of carboranes,⁴⁴ and the surface charge of the deposited ions is responsible for interparticle interactions, which resulted in the formation of a stable film.

Next, the surface structure of the ESD film was characterized using optical and electron microscopic techniques. Optical micrographs showed a sheet-like translucent appearance and the film was crumpled at multiple locations (Fig. 1c,

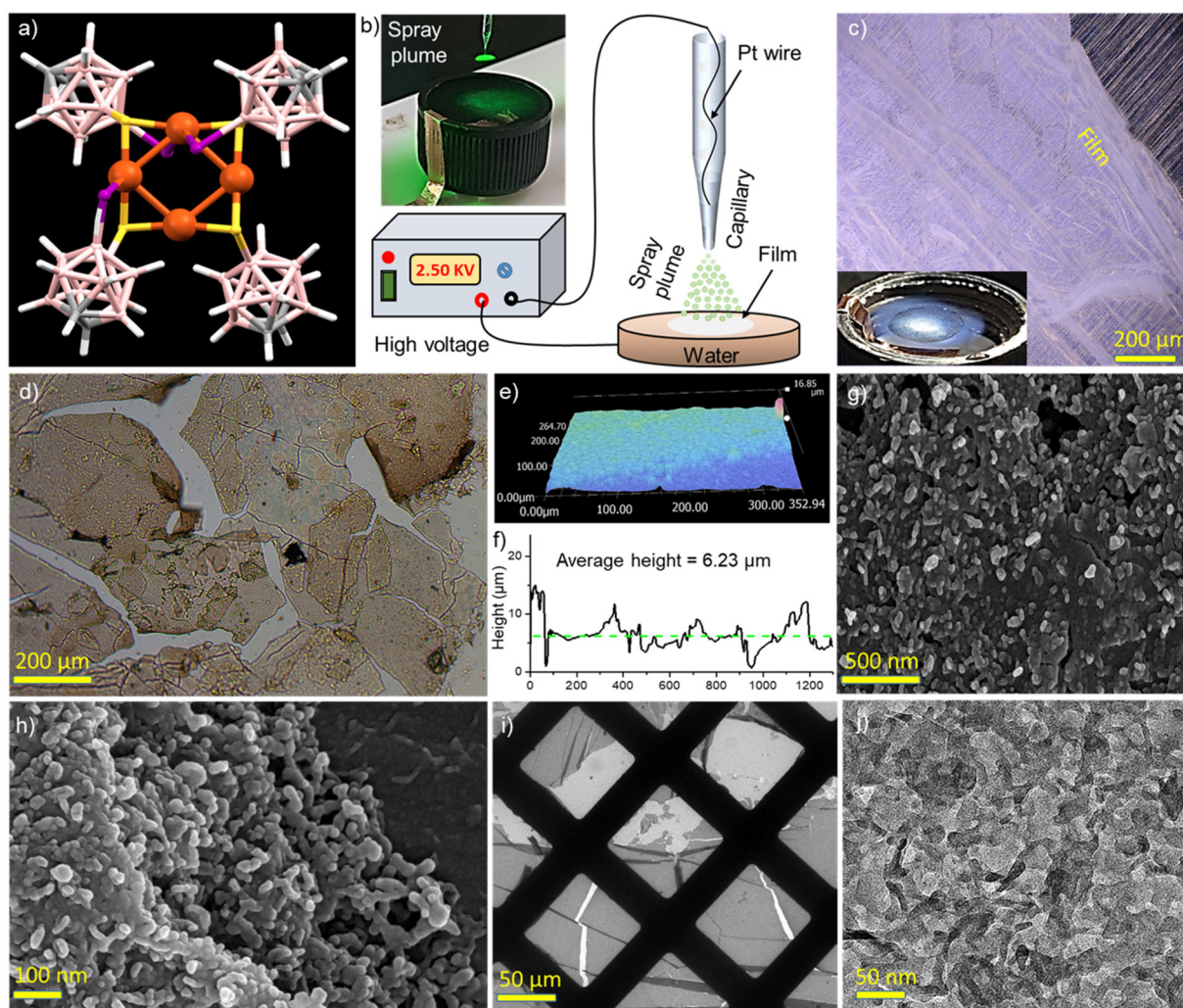


Fig. 1 (a) Molecular structure of the $\text{Cu}_4@$ ICBT cluster (atomic color code: orange = copper, yellow = sulphur, pink = boron, grey = carbon, violet = iodine and white = hydrogen). (b) Schematic representation of the ESD setup, (the inset shows the photograph of the spray plume during ESD, illuminated with a green laser). Electro spray deposition occurs on the surface of water, kept in a plastic cap, and the solution was grounded electrically. Optical micrographs of the film in (c) reflection and (d) transmission modes, respectively (the inset of (c) shows the floated film on the water surface). (e) 3D surface topology of the film indicating its roughness and (f) cross-section analysis. (g and h) FESEM micrographs and (i and j) TEM micrographs of the film at different magnifications.

d and S3[†]). Scratches on the aluminium substrate were visible through the film, indicating its translucent character. The surface topography reveals a relatively rough surface of the film (Fig. 1e) with an average thickness of 6.23 μm. We have used a scanning electron microscope to get additional information on its morphology. FESEM micrographs demonstrated (Fig. 1g and h) that the basal plane is covered by several fibrous knots. To understand the growth of the film, we measured the images after various deposition times, which revealed the formation of porous spherical aggregates after 10–15 min of deposition. As-formed spherical particles resulted in a compact film upon subsequent deposition process (Fig. S4[†]). The rough surfaces of the spherical aggregates with multiple tangles interact with each other and form the resulting film, which also has similar knots on its surface. Transmission electron micrographs (shown in Fig. 1i, j and S5[†]) confirm the sheet-like nanostructures with multiple knots. Thin film XRD (shown in Fig. S6[†]) reveals two broad diffraction peaks at 2θ values of 8.65° and 23.15°, suggesting the weak crystallinity of the film.

The molecular structure of the cluster in the film was verified using high-resolution electrospray ionization mass spectrometry (HRESI-MS). The MS spectrum of an acetone solution of the film (Fig. 2a) shows a characteristic peak at *m/z* 1334.02 with a monopositive charge. Experimental isotopic distribution of the mass having a molecular composition of [Cu₄S₄I₃(C₂B₁₀H₁₁)₄]₂H⁺ matches well with the calculated one (shown in the inset of Fig. 2a) and the parent cluster.⁴⁰ X-ray

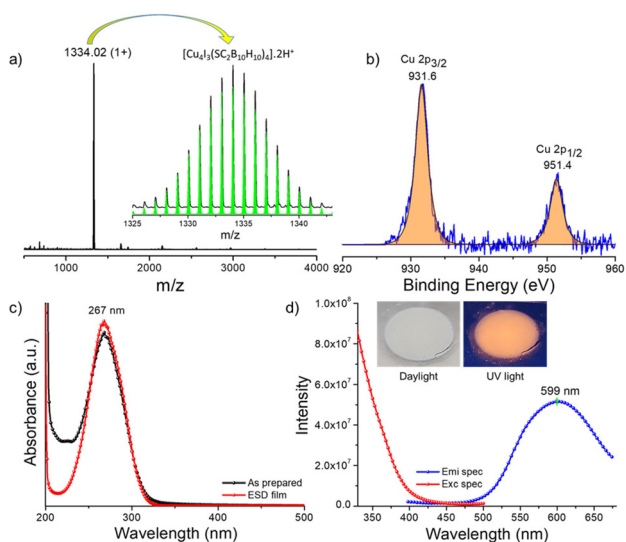


Fig. 2 (a) Positive ion-mode ESI-mass spectrum of a solution of the Cu₄@ICBT film in acetone. 0.1 (M) formic acid was added to increase the ionization efficiency. The inset shows the isotopic distribution of the experimental spectrum in comparison with the theoretical one. The spectrum is compared with the parent cluster. (b) Selected area XPS spectrum of the Cu 2p region. (c) UV-vis absorption spectra of the ESD film dissolved in acetone in comparison with the as-prepared cluster. (d) Photoluminescence excitation and emission spectra of the film. The inset shows the photograph of the ESD film under daylight (left) and UV light (right).

photoelectron spectroscopy (XPS) confirms the elemental composition (presence of Cu, S, C, B and I) in the film (Fig. S7[†]). Peak fittings of the Cu 2p region having two peaks at binding energies of 931.6 and 951.4 eV for 2p_{3/2} and 2p_{1/2} indicate a nearly zero oxidation state for copper (Fig. 2b). The UV-vis spectra of the film showed a single absorption band with a maximum of 267 nm, which is identical to that of the as-prepared cluster (Fig. 2c). All these data verified the essential structural stability of the cluster after the ESD process.

The as-grown ESD film emits bright orange luminescence under a 365 nm UV lamp. The solid state photoluminescence spectra of the film show a characteristic emission band centred at 599 nm under excitation at 330 nm (shown in Fig. 2d). The excitation and emission spectra compare well with the spectra of the parent cluster.⁴⁰ The Stokes shift of ~3.7 eV represents a large gap between the absorption and emission bands. Based on the molecular structure of the cluster with characteristic luminescence, we expected the material to function as a potential sensor of volatile organic compounds and thus we exposed the film to different organic solvents and nitroaromatics. While the characteristic orange luminescence remained unchanged after the film's exposure to vapours of various organic solvents, we observed a relatively quick quenching of the emission as a result of the film exposure to nitroaromatics (2-NT) with a vapour concentration of 0.024% at 25 °C (vapour pressure: 0.185 mm Hg). It took typically a few minutes to completely quench the emission. PL measurements show the complete disappearance of the 599 nm emission band after exposure to 2-NT (Fig. 3a) and its full recovery upon heating to 50 °C. The PL spectrum with a strong emission band confirmed the recovery (Fig. 3a). The

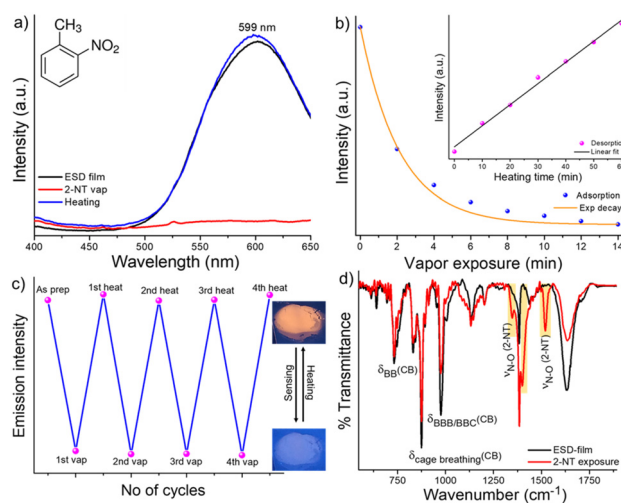


Fig. 3 (a) PL emission spectra of the film after 2-NT vapour exposure resulted in quenching the emission and thermal desorption (upon heating at 50 °C) resulted in the regeneration of luminescence. (b) Adsorption and desorption patterns of 2-NT from the film. (c) 2-NT vapour adsorption and desorption up to the 4th cycle, indicating the re-usability of the film. (d) Expanded FT-IR spectral region of the 2-NT-exposed film in comparison with the as-grown film. New features are highlighted.

stability of the clusters present in the ESD film after a complete adsorption and desorption cycle was monitored through MS studies by dissolving it in acetone. The appearance of the characteristic peak at m/z 1334.16 suggests the structural stability of the cluster after 2-NT adsorption and desorption processes (Fig. S8†).

To understand the kinetics of the adsorption and desorption processes, we measured the time-dependency of the emission features (shown in Fig. S9†), and we observed ~ 3 and 4.5-fold intensity reduction after 2 and 4 minutes of 2-NT exposure, respectively. The PL quenching of the film upon its exposure to 2-NT was exponential with no emission at all observed after ~ 15 min (Fig. 3b). The desorption of 2-NT by heating to 50 °C showed linear dependency and full luminescence recovery in ~ 60 min. The desorption process is slower than the adsorption process, which suggests a relatively strong interaction between the molecules of 2-NT and the film. Such types of adsorption and desorption processes indicate rapid adsorption and systematic desorption of 2-NT from the ESD film. Alternating exposure of the film to 2-NT vapours and thermal heating (Fig. 3c) demonstrated perfect reversibility of the adsorption–desorption process and PL measurements proved quantitative recovery of the luminescence properties.

Infrared (IR) and XPS measurements were performed to confirm the binding of 2-NT to the ESD film. IR spectra (shown in Fig. 3d and S10†) reveal the appearance of two new

vibrational peaks at 1347 and 1520 cm^{-1} due to N–O stretching modes, indicating the adsorption of 2-NT by the film. These features were absent for the parent film. Other characteristic vibrational peaks for C–H (3051 cm^{-1}) and B–H (2610 cm^{-1}) stretching modes, cage breathing mode (872 cm^{-1}), and BBB/BBC bending mode (975 cm^{-1}) of carboranes suggest the structural integrity of the cluster after 2-NT adsorption. Furthermore, the XPS study reveals the appearance of all the respective elements of the cluster, *i.e.*, Cu, S, C, B, and I, in the survey spectrum (Fig. S11†). We have observed two new peaks of N 1s and O 1s at the binding energy values of 405.3 and 531.9 eV, respectively.

The adsorption capacity of a microcrystalline $\text{Cu}_4\text{@ICBT}$ sample to 2-NT was tested using a uniform microcrystalline powder of the cluster. An optical micrograph reveals that the sample has rhombohedral microcrystals with dimensions of 20–25 μm length and 5–8 μm width (Fig. S12†). After dispersing these particles in DCM, we dropped them on a glass slide to make a thin film. In the subsequent step, this film of microcrystals was exposed to 2-NT (Fig. S12†). Time-dependent PL measurements showed nearly identical emission intensity even after 6 h of exposure. These results prove that the microcrystals themselves are incapable of 2-NT adsorption and detection, whereas the 2D film, prepared by ESD, with an exposed surface with characteristic morphologies promotes effective 2-NT adsorption.

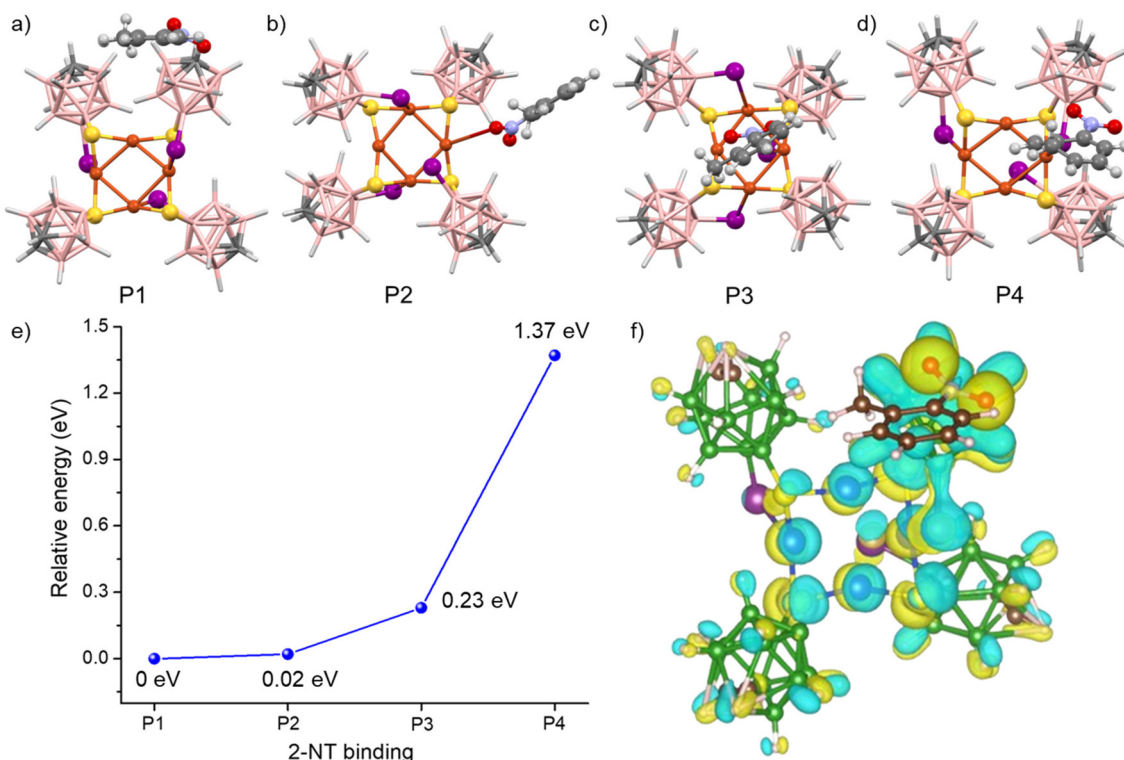


Fig. 4 (a–d) Structural representations of different binding configurations of 2-NT at different positions of the cluster. (e) Relative energy diagram of the binding of 2-NT with the respective position of $\text{Cu}_4\text{@ICBT}$. (f) Charge density difference (CDD) analysis of 2-NT binding with the cluster. Atomic color code used for the CDD plot is blue-copper, yellow-sulphur, green-boron, grey-carbon, and pink-hydrogen. The yellow and cyan electron density isosurfaces are plotted at a value of $0.005 \text{ eV } \text{\AA}^{-3}$.

Density functional theory (DFT) calculations using the Vienna *Ab initio* Simulation Package (VASP) were used to simulate the binding of 2-NT to the cluster.⁴⁵ The Cu₄@ICBT structure optimized using the Perdew–Burke–Ernzerhof (PBE) functional within the generalized gradient approximation (GGA) is given in Fig. S13.†⁴⁶ Details of the theoretical calculations are presented in the ESI.† This was followed by simulations of 2-NT binding at the Cu₄@ICBT optimized structure. Four positions, *i.e.*, (P1) parallel to carboranes, (P2) perpendicular to carboranes through the –NO₂ end, (P3) perpendicular to the Cu₄S₄ kernel, and (P4) parallel to the Cu₄S₄ kernel, were identified as most probable binding configurations (shown in Fig. 4a–d). DFT calculations proved that the P1 and P2 positions to be the most favourable binding positions having the lowest relative energies (RE) of 0 and 0.02 eV, respectively, whereas the P3 and P4 positions showed higher relative energy values of 0.23 and 1.37 eV. For the P1 binding configuration, the optimized geometry shows four intermolecular van der Waals interactions, *i.e.*, CH...HB, NO...B, NO...C, and NO...HC between the nitro group of the 2-NT molecule and a nearby carborane unit with distances of 2.39, 3.51, 3.21 and 2.43 Å, respectively (shown in Fig. S14†). For the P2 configuration, two strong interactions, *i.e.*, BH...N and BH...ON with the distances of 2.72 and 2.54 Å, respectively, showed favourable interactions between the two moieties (Fig. S15†). A similar type of strong intermolecular interactions between 2-NT with the cluster was not observed for any of the other configurations. Charge density difference (CDD) analysis shows that there is a delocalization of electron density between 2-NT and the cluster, resulting in feasible adsorption. Excited state charge transfer between the delocalized electron density of the LUMO of the cluster and 2-NT is assumed to be the driving force behind the emission quenching, upon its adsorption.

Freshly prepared films were independently exposed to various organic solvents to check the selectivity. The combined PL data (shown in Fig. S16–S26† and Fig. 5) showed comparable emission intensity of the film after its exposure to DCM, chloroform, methanol, ethanol, hexane, cyclohexane, benzene, toluene, acetonitrile, THF, and ethyl acetate vapours. However, complete luminescence quenching of the film was observed upon its exposure to two other nitroaromatics, 2,4-dinitrotoluene and picric acid (Fig. S27 and S28†), which proves the interesting selectivity of the film towards species with nitro functionality. Due to the lower vapour pressure, 2,4-dinitrotoluene and picric acid took ~30–35 min for complete luminescence quenching. Interactions between the nitro groups with the cluster are probably the reason behind luminescence quenching, which was also confirmed by DFT calculations.

In conclusion, this work demonstrated the fabrication of a film of atomically precise cluster functioning as a selective and reversible nitroaromatic vapour sensor using a molecularly flat carborane-thiol-protected tetranuclear copper nanocluster. The film was grown under an ambient condition through the ESD technique, depositing charged microdroplets of the clusters on water. Different microscopic techniques demonstrated the flexible nature of the film with surface porosity. Visible orange

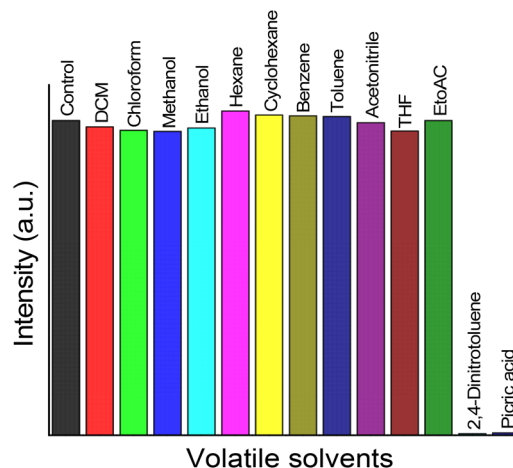


Fig. 5 Bar diagram shows the selectivity of the Cu₄@ICBT film to the exposed vapours (exposure time 2 h each) of various organic solvents and other nitro aromatic compounds, *i.e.*, 2,4-dinitrotoluene and picric acid. Luminescence quenching was observed only for nitroaromatics.

luminescence of the cluster was retained after the formation of the film. The as-grown film acts as a luminescence vapour sensor for detecting various nitroaromatics with excellent selectivity and full recovery of its luminescence by heating to only 50 °C. Theoretical calculations revealed favourable van der Waals interactions between the peripheral carboranes and the nitro moiety of the nitroaromatic species as responsible for luminescence quenching. Such a type of selective luminescence recognition has great potential for efficient visible detection of the precursors of explosives based on nitroaromatics. The extent of the sensitivity of the cluster-based sensor needs to be evaluated.

Conflicts of interest

There are no conflicts to declare.

Acknowledgements

The authors acknowledge the Department of Science and Technology (DST), Government of India, and the Ministry of Education, Youth and Sports of Czech Republic for financial support to the bilateral research projects DST/INT/Czech/P-16/2020 and LTAIN19152, respectively. A. J. acknowledges the financial support from IIT Madras. The authors acknowledge Papri Chakraborty and Jayoti Roy for their assistance with the mass spectrometry measurements. T. P. acknowledges funding from the Centre of Excellence (COE) on Molecular Materials and Functions under the Institution of Eminence scheme of IIT Madras. This work is a part of an India-Czech collaboration established by T. Pradeep and T. Base to explore the potential of carborane and metal clusters.

References

- X. Sun, Y. Wang and Y. Lei, *Chem. Soc. Rev.*, 2015, **44**, 8019–8061.
- S. Shanmugaraju and P. S. Mukherjee, *Chem. Commun.*, 2015, **51**, 16014–16032.
- R. Paolesse, S. Nardis, D. Monti, M. Stefanelli and C. Di Natale, *Chem. Rev.*, 2017, **117**, 2517–2583.
- P. Sulzer, A. Mauracher, S. Denifl, F. Zappa, S. Ptasinska, M. Beikircher, A. Bacher, N. Wendt, A. Aleem, F. Rondino, S. Matejcek, M. Probst, T. D. Mäk and P. Scheier, *Anal. Chem.*, 2007, **79**, 6585–6591.
- A. Chou, E. Jaatinen, R. Buividas, G. Seniutinas, S. Juodkakis, E. L. Izake and P. M. Fredericks, *Nanoscale*, 2012, **4**, 7419–7424.
- T. H. Kim, B. Y. Lee, J. Jaworski, K. Yokoyama, W. J. Chung, E. Wang, S. Hong, A. Majumdar and S. W. Lee, *ACS Nano*, 2011, **5**, 2824–2830.
- A. Chowdhury and P. S. Mukherjee, *J. Org. Chem.*, 2015, **80**, 4064–4075.
- D. Banerjee, Z. Hu and J. Li, *Dalton Trans.*, 2014, **43**, 10668–10685.
- Y. Zhang, M. Xu, B. R. Bunes, N. Wu, D. E. Gross, J. S. Moore and L. Zang, *ACS Appl. Mater. Interfaces*, 2015, **7**, 7471–7475.
- K. K. Kartha, S. S. Babu, S. Srinivasan and A. Ajayaghosh, *J. Am. Chem. Soc.*, 2012, **134**, 4834–4841.
- L. Lin, M. Rong, S. Lu, X. Song, Y. Zhong, J. Yan, Y. Wang and X. Chen, *Nanoscale*, 2015, **7**, 1872–1878.
- A. Mathew, P. R. Sajanlal and T. Pradeep, *Angew. Chem.*, 2012, **124**, 9734–9738.
- R. Jin, C. Zeng, M. Zhou and Y. Chen, *Chem. Rev.*, 2016, **116**, 10346–10413.
- I. Chakraborty and T. Pradeep, *Chem. Rev.*, 2017, **117**, 8208–8271.
- A. Mathew and T. Pradeep, *Part. Part. Syst. Charact.*, 2014, **31**, 1017–1053.
- X. Kang and M. Zhu, *Chem. Soc. Rev.*, 2019, **48**, 2422–2457.
- Atomically Precise Metal Nanoclusters*, ed. T. Pradeep, Elsevier, Amsterdam, 2023.
- J. Troyano, F. Zamora and S. Delgado, *Chem. Soc. Rev.*, 2021, **50**, 4606–4628.
- S. Perruchas, C. Tard, X. F. Le Goff, A. Fargues, A. Garcia, S. Kahlal, J. Y. Saillard, T. Gacoin and J. P. Boilot, *Inorg. Chem.*, 2011, **50**, 10682–10692.
- I. Roppolo, E. Celasco, A. Fargues, A. Garcia, A. Revaux, G. Dantelle, F. Maroun, T. Gacoin, J. P. Boilot, M. Sangermano and S. Perruchas, *J. Mater. Chem.*, 2011, **21**, 19106–19113.
- Z. Wu, J. Liu, Y. Gao, H. Liu, T. Li, H. Zou, Z. Wang, K. Zhang, Y. Wang, H. Zhang and B. Yang, *J. Am. Chem. Soc.*, 2015, **137**, 12906–12913.
- M. Xie, C. Han, Q. Liang, J. Zhang, G. Xie and H. Xu, *Sci. Adv.*, 2019, **5**, 1–9.
- W. A. Dar, A. Jana, K. S. Sugi, G. Paramasivam, M. Bodiuzzaman, E. Khatun, A. Som, A. Mahendranath, A. Chakraborty and T. Pradeep, *Chem. Mater.*, 2022, **34**, 4703–4711.
- M. E. Germain and M. J. Knapp, *Chem. Soc. Rev.*, 2009, **38**, 2543–2555.
- Y. Wang, A. La, Y. Ding, Y. Liu and Y. Lei, *Adv. Funct. Mater.*, 2012, **22**, 3547–3555.
- Z. Luo Jr., A. W. Castleman and S. N. Khanna, *Chem. Rev.*, 2016, **116**, 14456–14492.
- Q. Yao, Z. Wu, Z. Liu, Y. Lin, X. Yuan and J. Xie, *Chem. Sci.*, 2021, **12**, 99–127.
- J. Cyriac, T. Pradeep, H. Kang, R. Souda and R. G. Cooks, *Chem. Rev.*, 2012, **112**, 5356–5411.
- S. Rauschenbach, F. L. Stadler, E. Lunedei, N. Malinowski, S. Koltsov, G. Costantini and K. Kern, *Small*, 2006, **2**, 540–547.
- Z. Wu, J. Liu, Y. Li, Z. Cheng, T. Li, H. Zhang, Z. Lu and B. Yang, *ACS Nano*, 2015, **9**, 6315–6323.
- S. Chandra, Nonappa, G. Beaune, A. Som, S. Zhou, J. Lahtinen, H. Jiang, J. V. I. Timonen, O. Ikkala and R. H. A. Ras, *Adv. Opt. Mater.*, 2019, **7**, 1900620.
- (a) M. Jash, A. Jana, A. K. Poonia, E. Khatun, P. Chakraborty, A. Nagar, T. Ahuja, K. V. Adarsh and T. Pradeep, *Chem. Mater.*, 2023, **35**, 313–326; (b) Z. Xie, P. Sun, Z. Wang, H. Li, L. Yu, D. Sun, M. Chen, Y. Bi, X. Xin and J. Hao, *Angew. Chem., Int. Ed.*, 2020, **59**, 9922–9927.
- Z. Wu, C. Dong, Y. Li, H. Hao, H. Zhang, Z. Lu and B. Yang, *Angew. Chem., Int. Ed.*, 2013, **52**, 9952–9955.
- V. Hynninen, S. Chandra, S. Das, M. Amini, Y. Dai, S. Lepikko, P. Mohammadi, S. Hietala, R. H. A. Ras, Z. Sun, O. Ikkala and Nonappa, *Small*, 2021, **17**, 2005205.
- D. Sarkar, M. K. Mahitha, A. Som, A. Li, M. Wlekinski, R. G. Cooks and T. Pradeep, *Adv. Mater.*, 2016, **28**, 2223–2228.
- A. Jana, S. K. Jana, D. Sarkar, T. Ahuja, P. Basuri, B. Mondal, S. Bose, J. Ghosh and T. Pradeep, *J. Mater. Chem. A*, 2019, **7**, 6387–6394.
- A. Jose, A. Jana, T. Gupte, A. S. Nair, K. Unni, A. Nagar, A. R. Kini, B. K. Spoorthi, S. K. Jana, B. Pathak and T. Pradeep, *ACS Mater. Lett.*, 2023, **5**, 893–899.
- A. R. Chowdhuri, B. K. Spoorthi, B. Mondal, P. Bose, S. Bose and T. Pradeep, *Chem. Sci.*, 2021, **12**, 6370–6377.
- J. Ghosh and R. G. Cooks, *TrAC, Trends Anal. Chem.*, 2023, **161**, 117010.
- A. Jana, M. Jash, W. A. Dar, J. Roy, P. Chakraborty, G. Paramasivam, S. Lebedkin, K. Kirakci, S. Manna, S. Antharjanam, J. Machacek, M. Kucerakova, S. Ghosh, K. Lang, M. M. Kappes, T. Base and T. Pradeep, *Chem. Sci.*, 2023, **14**, 1613–1626.
- J. Li, H. Z. Ma, G. E. Reid, A. J. Edwards, Y. Hong, J. M. White, R. J. Mulder and R. A. J. O'Hair, *Chem. – Eur. J.*, 2018, **24**, 2070–2074.
- (a) N. Yan, N. Xia and Z. Wu, *Small*, 2020, **200609**, 1–9; (b) X. Kang, H. Chong and M. Zhu, *Nanoscale*, 2018, **10**, 10758–10834.
- (a) X. Kang and M. Zhu, *Chem. Mater.*, 2019, **31**, 9939–9969; (b) M. S. Bootharaju, V. M. Burlakov, T. M. D. Besong,

- C. P. Joshi, L. G. Abdulhalim, D. M. Black, R. L. Whetten, A. Goriely and O. M. Bakr, *Chem. Mater.*, 2015, **27**, 4289–4297; (c) A. Jana, P. M. Unnikrishnan, A. K. Poonia, J. Roy, M. Jash, G. Paramasivam, J. Machacek, K. N. V. D. Adarsh, T. Base and T. Pradeep, *Inorg. Chem.*, 2022, **61**, 8593–8603.
- 44 S. Fujii, *Med. Chem. Commun.*, 2016, **7**, 1082–1092.
- 45 G. Kresse and J. Hafner, *Phys. Rev. B: Condens. Matter Mater. Phys.*, 1994, **49**, 14251–14269.
- 46 G. Kresse and D. Joubert, *Phys. Rev. B: Condens. Matter Mater. Phys.*, 1999, **59**, 1758–1775.